MAPAN-JOURNAL ,
Publisher: METROLOGY SOC INDIA , NPL PREMISES,
Address: DR K S KRISHNAN MARG, NEW DELHI, INDIA,
ISSN / eISSN:0970-3950 / 0974-9853
Volume 25-Issue 1-(2025)
DOI:https://doi-001.org/1025/17736553877884

# Macrophage dysfunction in diabetic wound healing: the role of Keap1/Nrf2-Nlrp3 signaling in immune regulation

Linian Peng [1,2], Zhihui Liu [1,2], Yong Huang [1,2], Weifeng He [1,2]*

[1] State Key Laboratory of Trauma, Burn and Combined Injury, Institute of Burn Research, Southwest Hospital, Third Military Medical University (Army Medical University), 400000, Chongqing, China;

[2] Department of Disease Proteomics, Chongqing Key Laboratory for Disease Proteomics, 400000, Chongqing, China;

*Correspondence： Weifeng He (whe761211@hotmail.com)

## Abstract

**Objectives:** To elucidate the pathophysiologic mechanism of diabetic wounds that are difficult to heal, investigate the dysfunctional role of macrophages in diabetic wound healing , and explore new mechanisms and therapeutic targets for the pathogenesis of diabetes mellitus (DM).

**Methods:** Streptozotocin (STZ) induced type I diabetic mice were generated, a full-thickness dorsal skin wound model was established in micefor gross observation, traumatic tissues were collected for paraffin section staining， primary macrophages were isolated from mice,a cell culture model combining high glucose and impaired glucose utilization (2DG treatment) was established to mimic diabetic conditions, and the expression of phagocytosis, oxidative stress (OS), inflammatory proteins, and polarization and apoptosis genes was quantified via immunofluorescence (IF), immunohistochemistry (IHC), real time fluorescence quantitative polymerase chain reaction (RTFQ-PCR) and western blotting (WB) technology.

**Results:** Compared with those in the normal group, in the diabetic group, wound healing was slow, phagocytosis was diminished, OS was excessive, macrophage polarization was unbalanced, and the inflammatory response was excessive.

**Conclusions:** Impaired diabetic wound healing is attributed to high glucose induced macrophage dysfunction. Inhibition of phagocytosis, M1/M2 polarization imbalance, kelch like ech associated protein 1 (Keap1)/nuclear factor erythroid 2 related factor 2(Nrf2) nod like receptor thermal protein domain associated protein 3(Nlrp3) mediated OS-inflammation cycle, and endocytosis defects. Therapeutic strategies such as Nrf2 activators, Il-1 β

antagonists, and bionic dressings are promising. Further exploration of the interaction between Nrf2 and inflammation is needed to personalize therapy.

**Keywords:** Diabetic wound healing; macrophage dysfunction; oxidative stress.

## Key message:

**Research on this topic has shown that** diabetic wound healing is chronic, with a disturbed wound healing environment that is inconsistent with the process of healing wounds under physiological conditions.

**This study presents** the first dual metabolic disorder model of high glucose and 2DG, revealing the triple defects of macrophage phagocytosis, polarization, and inflammation, as well as the vicious cycle of Keap1/Nrf2-Nlrp3. It proposes a targeted intervention strategy.

**How this study might affect research, practice or policy:**

This study identifies new targets for diabetic wound treatment, advances personalized medicine, and extends to other complications.

## Introduction

Skin tissue repair is a complex process vital for defence and homeostasis [1,2]. Injuries such as burns, diabetic ulcers, and combat wounds heal slowly because of intricate mechanisms [3,4]. In China, chronic diabetic wounds outnumber common traumatic wounds, and current treatments are costly and ineffective, necessitating new strategies [5,6]. Wound healing involves overlapping mechanisms, including phagocytosis, oxidative stress (OS), and inflammation. Diabetic wounds exhibit an impaired microenvironment, including OS and dysregulated inflammatory responses, but the underlying mechanisms remain unclear and require further study.

Wound healing is generally divided into four overlapping phases: hemostasis, inflammation,

proliferation, and remodeling， with macrophages playing a central role [7]. Initially, platelets activate coagulation, releasing growth factors to establish the healing microenvironment [8,9]. Neutrophils then trigger inflammation, recruiting monocytes that differentiate into macrophages [10,11]. These macrophages secrete bioactive molecules that activate fibroblasts, endothelial cells, and keratinocytes [12]. During proliferation, macrophages promote angiogenesis through the vascular endothelial growth factor (VEGF), while fibroblasts synthesize the extracellular matrix [7,19]. Later, M1 macrophages shift to the M2 type, reducing inflammation and facilitating tissue repair [11,20]. Macrophages recognize damage associated molecular patterns (DAMPs) and pathogen associated molecular patterns (PAMPs) through pattern recognition receptors (PRRs) to initiate nonspecific immune responses [21-23]. In diabetes mellitus (DM), macrophages are impaired in various biological functions, the mechanisms of which require further exploration.

This study reveals new mechanisms underlying diabetic wound healing disorders, suggesting that macrophage dysfunction may be a key target, and discovers new pathogenic mechanisms and therapeutic targets.

## Materials and methods

### mice and skin creation

Male C57BL/6J wild type（WT） mice, 6-8 weeks old and weighing approximately 20 g, were provided by the Experimental Center of Army Military Medical University and housed in the Experiment Center of Southwest Hospital. The mice were fasted and dehydrated for 12 hours(h) before the experiment. The experimental group was then injected intraperitoneally with 120 mg/kg streptozotocin (STZ) in citrate buffer to potential of hydrogen（pH）4.5. The control group was injected with an equal amount of buffer for 3 day, and those with tail vein blood glucose levels greater than 16.7 mmol/l, measured after 1 week, were considered the experimental group. Both groups were anesthetized with 1% sodium pentobarbital at a dose of 7.5 ml/kg. Two 6 mm circular wounds were created after dorsal hair removal, and the animals were housed in a single cage. The wounds were photographed and recorded on days 0, 2, 4, 6, and 8 using a 3M adhesive ring scale. The degree of epithelialization of the traumatic histopathological structures was observed, including the measurement of the thickness and length of the neoplastic epithelium and the percentage of healed area of the trauma, healed area of the trauma (%) = 1 - unhealed area X 100%. The data were analyzed via ImageJ software.

### Tissue sampling and paraffin sectioning

Tissues were collected from the traumatic surfaces of the mice in the model and control groups on days 2, 4, 6 and 8 after trauma. After anesthesia, the skin was cut at a distance of 3 mm from the trauma edge, and the subcutaneous tissue was removed and fixed in five volumes of 4%

paraformaldehyde solution at 4°C for 48 h. The tissue was subsequently dehydrated, clarified, embedded in paraffin wax, sectioned into 5 μm slices, and spread on slides in a water bath at 40°C. The slides were then labelled for drying at room temperature for 1 h and subsequently preserved at 4°C.

**Paraffin section staining**

The paraffin embedded sections were heated at 60°C for 20 minutes (min) after routine dewaxing: (1) hematoxylin and eosin (H&E) staining: H&E staining, followed by dehydration and sealing; (2) masson staining: iron hematoxylin staining, hydrochloric acid alcohol differentiation, aniline blue coloring for 10 min, washing and sealing; (3) immunohistochemistry (IHC): after antigen repair, the endogenous enzyme was blocked, the samples were blocked for 20 min, the primary antibody (1:200, Abcam, UK) was added overnight at 4°C, biotin-labeled goat anti-rabbit IgG was added for 15 min, horseradish peroxidase labeled streptavidin（SA-HRP）working solution was added dropwise, and dolichos biflorus agglutinin (DAB) coloring was performed.

**Cell isolation and processing**

The femurs and tibias of 6-8 week old C57BL/6J WT mice were removed, the muscle was removed after sterilization with 75% alcohol, and the bone marrow was rinsed with phosphate buffered saline (PBS), filtered at 0.45 μm, and centrifuged at 1500 × g for 5 min. The cells were inoculated at $2\times10^6$/well in roswell park memorial institute 1640(RPMI1640) medium (Thermo Fisher, USA) containing 20 ng/ml macrophage colony stimulating factor (MCSF) (ABclonal, CHN), 100 μg/ml penicillin streptomycin amphotericin B mixture (Solarbio, CHN) and 10% fetal bovine serum (FBS) (Thermo Fisher, USA) in RPMI 1640 medium and cultured at 37°C with 5% $CO_2$ for 5 days to induce bone marrow derived macrophages(BMDMs) maturation. On 5 day, the mature primary macrophages were washed with PBS and divided into the following groups: (1) the 10 mM glucose group, the 10 mM glucose plus 2 deoxy D glucose (2DG) group, the 17.5 mM glucose group and the 17.5 mM glucose plus 2DG group. (2) The above four groups were repeated with 100 ng/ml interleukin-4 (Il-4) or 40 ng/ml lipopolysaccharide (LPS). Each group was treated with 1 ml of medium/well for 24 h at 37°C, 95% humidity and 5% $CO_2$ in a low oxygen incubator.

**Cell immunofluorescence (IF)**

The treated mature primary macrophages were washed three times with phosphate buffers aline (PBS) for 5 min each time, then discarded, and fixed with 4% paraformaldehyde for 15-30 min at room temperature. The samples were then blocked with primary antibody blocking solution (Beyotime, CHN) for 2 h at room temperature and then incubated with a wet cassette primary antibody at 4°C overnight, followed by cluster of differentiation (CD)86, inducible nitric oxide synthase (iNOS), CD206, and arginase 1 (Arg1) (1:200; Abcam, UK). The next day ,the wet cassette was incubated at room temperature for 30 min. Then, the samples were incubated with secondary

antibodies AF488 and AF555 (1:1000; Abcam, UK) for 1 h at room temperature, and 4′,6-diamidine-2′-phenylindole dihydrochloride (DAPI) (Beyotime, CHN) was added dropwise. The nuclei were stained for 5 min, then blocked, and visualized using an inverted fluorescence microscope with a 20X magnification.

**Real time fluorescence quantitative polymerase chain reaction (RTFQ-PCR)**

Total RNA was extracted from mature primary macrophages via RNAiso PULS (Takara Bio, CHN) reagent, and reverse transcription was performed via 2XSP qPCR Mix (Qianxi Biotechnology, CHN) and HiScript III RT SuperMix for qPCR (+gDNA wiper) (Vazyme, CHN) to synthesize cDNA, followed by RTFQ-PCR.mice adaptor protein（Ap）-1 forward primer 5'-ACTGGCATGAGAATGCCTCC-3' and reverse primer 5'-TTGGGGCACAAGCTTTCTGA-3'; mice AP-2 forward primer 5'-TGTATCCAAAGGCGATGGCA-3' and reverse primer 5'-AGCCTCTTTGCTCTCTTGCAGT-3'; mice AP-3 forward primer 5'-ACTGCTTCAACGTCACCCTC-3' and reverse primer 5'- GAGCGTTCCTTGCTCCTTCT-3 '; mice AP-4 forward primer 5'-CTTGCACAGTTTGCCAGGTC-3' and reverse primer 5'-CCTCCACCTTCTGGAGCTTG-3'; mice CD16 forward primer 5'-TGCACACTCTGGAAGCCAAT-3' and reverse primer 5'-CTCTGGGAAGCCAAT-3';mice CD32 forward primer 5'-ATGGGCTGTGATCGGAACTG-3' and reverse primer 5'-ACTGGCATGAGAATGCCTCC-3'; mice Il-1β forward primer 5'-GCCACCTTTTGACAGTGATG-3'and reverse primer 5'-TTGGAAGCAGCCCTTCATCTT-3'; mice Il-12 forward primer 5'-TGTGCAATCACGCTACCTCC-3' and reverse primer 5'-ATGACCCTGGCCAAACTGAG-3';mice Il-6 forward primer 5'-ACAAAGCCAGAGTCCTTCAGAG-3' and reverse primer 5'-TCTGTGACTCCAGCTTATCTCTTG-3';Il-10 forward primer 5'-TGTCATCGATTTCTCCCCTGTG-3' and reverse primer 5'-GCCTTGTAGACACCTTGGTCTT-3'; transforming growth factor-β （Tgf-β） forward primer 5'-AAAAGCAGTCAGCTGGCCTT-3' and reverse primer 5'-GCAATGCAGACGAAGCAGAC-3';reaction conditions: 95°C denaturation for 2 min; 95°C denaturation for 15 s, 55°C annealing for 35 s, and 72°C extension for 31 s, for a total of 40 cycles. The reactions were analyzed via the Bio-Rad CFX Manager 3.1 system software.

**Western blotting(WB) analysis**

Mature primary macrophages were processed, and RIPA lysis buffer was added to extract cellular proteins. A bicinchoninic acid (BCA) kit (Thermo Fisher, USA) was used to determine the protein concentration, and the number of proteins was adjusted. Then, 1X loading buffer (Yamay Biotech, CHN) was added, the mixture was boiled at 100°C for 10 min, and the proteins were separated via sodiumdodecyl sulfate polyacrylamide gel electrophoresis（SDS-PAGE） (Yamay

Biotech, CHN). 30 μg of sample volume was added per well. The upper gel voltage was set at 80 V, and the lower gel voltage was set at 100 V. The membrane was then transferred, and the mixture was incubated. A total of 30 μg of sample per well of sample mixture was used.The upper gel volume was 80 V, the gel volume was 100 V, the membrane was transferred, the primary antibody b cell lymphoma 2 (Bcl2) (1:1000, Abcam, UK),bcl2 associated x protein (Bax) (1:1000, Abcam, UK), nuclear factor erythroid 2 related factor 2 (Nrf2) (1:1000, ABclonal, CHN), nad(p)h:quinone oxidoreductase I(Noq1) (1:1000, ABclonal, CHN), kelch like ech associated protein 1 (Keap1) (1:1000, ABclonal, CHN), Il-1β (1:1000, Abcam, UK), and nod like receptor thermal protein domain associated protein 3 (Nlrp3) (1:1000, Abcam, UK), cysteine aspartate protease 1(Caspase1) (1:1000, Abcam, UK), and glyceraldehydes 3 phosphatedehydrogenase (Gadph ) (1:1000, Abcam, UK) at 4°C in the refrigerator, and the next day, tris borate sodium tween 20(TBST) was washed 5 times for 5 min，were incubated with goat anti-mousemice horseradish peroxidasehorseradish peroxidase (HRP) 2h.The results were analyzed via ImageJ software.

**Statistical analysis**

Data were obtained from at least three independent replicate experiments and represented as mean ± standard error of mean (SEM). Student’s two-tailed unpaired t-test to determine the significant differences using SPSS statistical software. A p value of $<0.05$ was considered statistically significant. Statistical graphs were generated using GraphPad Prism 9.0.0.

# Results

**The wound healing situation of mice, as well as H&E staining and Masson staining**

We established a diabetic mice whole skin defect model to observe differences in wound healing. On 2 day after trauma ,bleeding spots appeared under the scab in the diabetic group, and there was no bleeding in the normal group. On 4 day, the scab in the normal group thickened to a deep red color, and there was still scattered bleeding in the diabetic group. On 6 day, the scab was partially removed in the normal group, and the diabetic group showed persistent thick scab without epithelialization.On 8 day, the scab in the normal group was close to healing, with obvious epithelialization, while that in the diabetic group remained intact, showing no significant epithelialization (Figure 1A). A statistical analysis of the wound healing rate between the two groups revealed that there was no significant difference in the wound healing rate on 2 day after trauma, and there was a substantial difference on days 4, 6, and 8 after trauma (Figure 1B). Masson staining revealed that collagen deposition in the diabetic group was sparse and disarranged (Figure 1C).Compared with the control group, the area of collagen deposition in the diabetic group was significantly lower on days 4, 6, and 8(Figure 1D), and there was no difference on 2 day. HE staining

revealed that inflammatory cell infiltration was apparent and accompanied by neovascularization in the control group on 2 day, whereas the diabetic group had fewer neovascularizations. The dermis of the control group was dense, and the vasculature was mature on 4 day, whereas that of the diabetic group had sparse dermis and fewer vascularizations. Epithelialization was present in both groups on 6 day, but granulation tissue was more abundant in the control group, and the control group was more richly organized on 8 day. On 8 day, the trabeculae were filled, and inflammation subsided in the control group, whereas trabecular defects and persistent inflammation remained in the diabetic group (Figure 1E). Quantitative analysis revealed a significant difference in epithelial thickness between the two groups at all four time points; the difference in epithelial length was substantial at all time points except 2 day(Figure 1F, G).

**IHC staining of clathrin proteins**

In order to study the mechanism of abnormal wound phagocytosis, we detected the expression of clathrin in the wounds of the diabetic group and the control group on the 4 and 8 days. IHC showed that the expression of clathrin heavy chain (CHC) in the diabetic group increased with time. On the 4 day, the expression of CHC protein in the control group was three times that in the diabetic group, and the expression of clathrin in the diabetic group increased five times on the 8 day (Figure 2B, C). The expression of clathrin light chain (CLC) protein also tended to decrease in the control group. On the 4 day, the expression of clathrin light chain (CLC) protein in the control group was nearly twice that in the experimental group. On the 8 day, the expression of clathrin light chain (CLC) protein in the experimental group was twice that in the experimental group (Figure 2D, E). In diabetic tissues, the activation of CHC and CLC is delayed, which interferes with the normal wound healing process and prevents the timely clearance of necrotic substances.

**IHC staining of vascular markers, oxidative stress, and inflammasome**

IHC analysis of the expression of OS and inflammation related proteins in diabetic wounds revealed that the vascular marker CD31 increased over time in both groups, but the expression in the diabetic group was significantly lower than that in the control group (Figure 3A, B), suggesting impaired angiogenesis. Keap1 expression decreased in both groups but remained persistently high in the diabetic group (Figure 3C, D), suggesting that OS was abnormally regulated. Compared with the control group, the expression of the key antioxidant factor Nrf2 in the diabetic group was lower on 4 day and reversed on 8 day (Figure 3E, F), reflecting a late compensatory activation. The number of Nlrp3 inflammatory vesicles was significantly greater than that in the control group at both time points in the diabetic group (Figure 3G, H). These results suggest that diabetic wounds have impaired angiogenesis, dysregulation of the Keap1/Nrf2 pathway and persistent Nlrp3 inflammatory vesicle hyperactivation, which together lead to an imbalance between OS and the inflammatory response and impede wound healing.

**Stimulate primary macrophage polarization with IF staining**

To determine whether macrophage polarization was affected in DM, on the fifth day of primary macrophage maturation, we added IL-4 and LPS, placed them in a hypoxic incubator for 24 h at a serum concentration of 1%, and then grouped them into 10 mM, 10 mM plus 2DG, 17.5 mM, 17.5 mM plus 2DG, and four groups; prepared cell crawls; and used the cellular IF technique to measure the expression of target genes, CD86, iNOS, CD206, and Arg1. Compared with those in the 10 mM group, the expression of target proteins in the remaining three groups decreased to different degrees (Figure 4A, B).

**RTFQ-PCR technique is used to detect the expressions of adaptor proteins, phagocytic molecules and inflammatory factors.**

Total detected by real time fluorescence PCR, the expression of the clathrin articulating proteins AP-1, AP-2, AP-3, and AP-4 was significantly lower in the high glucose and 2DG groups than in the 10 mM group (Figure 5A), suggesting that diabetic environments impair clathrin mediated endocytosis (CME). Moreover, the expression of the phagocytic receptors CD16 and CD32 was significantly downregulated in the 17.5 mM plus 2DG group (Figure 5B, C), further confirming the impaired phagocytosis of macrophages. Another study revealed that the expression of the proinflammatory factors Il-6 and Il-1β was elevated in the 17.5 mM plus 2DG group, whereas the expression of the anti-inflammatory factors Il-10 and Tgf-β was significantly reduced (Figure 5E-I). These results indicate that macrophages in the diabetic environment exhibit phagocytic dysfunction, characterized by an imbalance between M1/M2 polarization, and that the overexpression of Il-6 and insufficient secretion of anti-inflammatory factors may be key mechanisms involved in maintaining pathological inflammation.

**Detection of cellular proteins by WB technique**

Protein blotting analysis revealed that high glucose combined with glucose metabolism inhibition in the 17.5 mM plus 2DG group significantly upregulated the expression of OS and inflammation related proteins, and the expression of Nlrp3 inflammatory vesicles, Caspase1, and Il-1β was greater than that in the normal 10 mM glucose group (Figure 6A, B). In addition, the expression of the proapoptotic proteins Bax/Bcl2 ratios was significantly elevated (Figure 6C, D), indicating increased apoptosis. These results suggest that the diabetic environment leads to, first, overactivation of OS; second, sustained activation of Nlrp3 inflammatory vesicles; and third, increased apoptosis. Together, these mechanisms lead to an uncontrolled inflammatory response, which is the key pathologic basis for the difficulty in healing diabetic wounds.

# Discussion

In diabetic wounds, moderate levels of reactive oxygen species (ROS) facilitate wound cleansing, but excessive levels cause cellular damage [24,25]. Chronic inflammation in DM impairs healing [26,27], with macrophages showing M1 polarization [28,29] and phagocytic dysfunction resulting from the accumulation of advanced glycation end products (AGEs) via epigenetic changes [30,31]. Additionally, impaired CME, which is crucial for pathogen clearance and signaling [29,30], further hinders repair, although its role in diabetic wounds remains poorly understood [32,33]. This reseach established a diabetic mice model to compare diabetic and routine wound healing and explore the underlying molecular mechanisms to guide clinical treatment. The findings revealed multiple impairments in the healing of diabetic wounds.

The length and thickness of the new epithelium are insufficient, collagen deposition and angiogenesis are significantly reduced, and the CD31 expression level is decreased, reflecting impaired neovascularization, resulting in an inadequate blood oxygen supply to the wound. Moreover, an abnormally increased OS and imbalance of the Keap1/Nrf2 pathway resulted in an increased inflammatory response and activation of Nlrp3 inflammatory vesicles, thereby delaying wound healing. In this study, we constructed an in vitro cellular model of high glucose combined with 2DG to simulate, for the first time, the dual disorders of cellular glucose metabolism in DM, hyperglycemia and impaired glucose utilization, and to investigate the mechanism underlying abnormal macrophage function. A comparative analysis of differences between DM and normal wound healing provides a theoretical basis for clinical treatment and intervention directions. Macrophages are significantly dysfunctional in the diabetic environment. The phagocytic capacity of macrophages is significantly impaired, and the expression of network proteins and phagocytic receptors, such as AP-1, AP-2, AP-3, and AP-4, decreases, which affects the clearance of pathogens and increases the risk of infection. Inflammatory factor expression is imbalanced, resulting in a pattern of "low Il-10, Tgf-β and high Il-6", disrupting the inflammatory-anti-inflammatory balance required for wound healing. Macrophages are less polarized and more inclined to convert to the M1 type, and the expression of M1/M2 markers is simultaneously decreased, which affects the tissue repair process. At the molecular level, the present study made several innovative discoveries. For the first time, a novel mechanism of interaction between OS and inflammation was revealed, confirming that an imbalance in the Keap1/Nrf2 pathway in the diabetic environment led to a decrease in antioxidant capacity, a reduction in Nqo1 expression, and an increase in Nlrp3 inflammatory vesicle activation, which resulted in the formation of a vicious cycle of "OS-inflammation" and aggravated tissue damage.

In addition, hyperglycemia alters the expression of the pro-apoptotic protein Bax and the anti-apoptotic protein Bcl2 by inhibiting Nrf2 nuclear translocation, thereby revealing the molecular pathways through which metabolic disorders regulate the fate of immune cells. Our study identified key therapeutic targets and clinical strategies for diabetic wound healing. Immune

modulation—correcting macrophage polarization or supplementing anti-inflammatory factors—restores wound homeostasis. Biomimetic dressings, which utilize clathrin endocytosis, enhance macrophage clearance of pathogens. A macrophage based prognostic system enables phased clinical interventions. Translational approaches include monitoring Keap1/Nrf2 ratios and Nlrp3 inflammasome activity, as well as combined antioxidant anti-inflammatory therapy and personalized immune metabolic treatment plans. Future research should elucidate the crosstalk between the Nrf2 inflammatory pathway and extend these findings to diabetic complications, refining therapeutic strategies to improve outcomes and reduce healthcare burdens.

In this research, we chose to adopt three independent experimental designs based on a comprehensive balance between various scientific considerations and the actual situation. First of all, from the perspective of research nature, this study aims to preliminarily verify the effects of macrophage dysfunction and Keap1/Nrf2-Nlrp3 signaling pathway on immunity in DM, and its core goal is to provide proof of concept for this field. The current limitation of our research is the lack of human data and the lack of long term wound healing assessment.The determination of sample size is subject to unavoidable ethical constraints. This study involves experimental animals, and the "3R principle" (replacement, reduction, optimization) must be followed in the acquisition process. Although there are sample size constraints on the existing data, its disclosure phenomenon and effect are highly reproducible.

## Conclusion

Diabetic wounds feature macrophage dysfunction due to Keap1/Nrf2-Nlrp3 dysregulation .In pathological conditions such as diabetes mellitus, the imbalance of the Keap1/Nrf2 pathway leads to the decline of antioxidant capacity and the reduction of Nqo1 expression. At the same time, the Nlrp3 inflammasome is overactivated, forming a vicious cycle of oxidative stress and inflammation and exacerbating tissue damage. Further studies are needed to elucidate the crosstalk between Nrf2 signaling and inflammasome activation, and promote personalized immunometabolic therapy and combination strategies by monitoring Keap1/Nrf2 ratio and Nlrp3 activity, so as to improve prognosis and reduce medical burden.Future research can extend the observation time by expanding the number of samples and introducing human organoids or clinical samples, so as to enhance the reliability of the results and clinical translation value.

## Availability of data and material

The data and supporting material are available upon request.

## Ethics declarations

Competing interests: the authors declare that they have no competing interests.

## Contributions

The cell experiments in this study were conducted using LNP and ZHL.LNP, and YH completed the animal experiments. The experimental project was proposed and planned by WFH.

## Acknowledgments

This work was supported by grants from the National Natural Sciences Foundation of China (No. 82172232 and No. 31872742 to WFH), the Military Medical Science and Technology Youth Training Program of the Army MIiltary Medical University (Third Military Medical University) (No. 20QNPY024 to WFH) and the Special Project for Enhancing Science and Technology Innovation Ability (frontier exploration) of the Army Miltary Medical University (Third Military Medical University) (No. 2019XQY12 to WFH).

## Legends

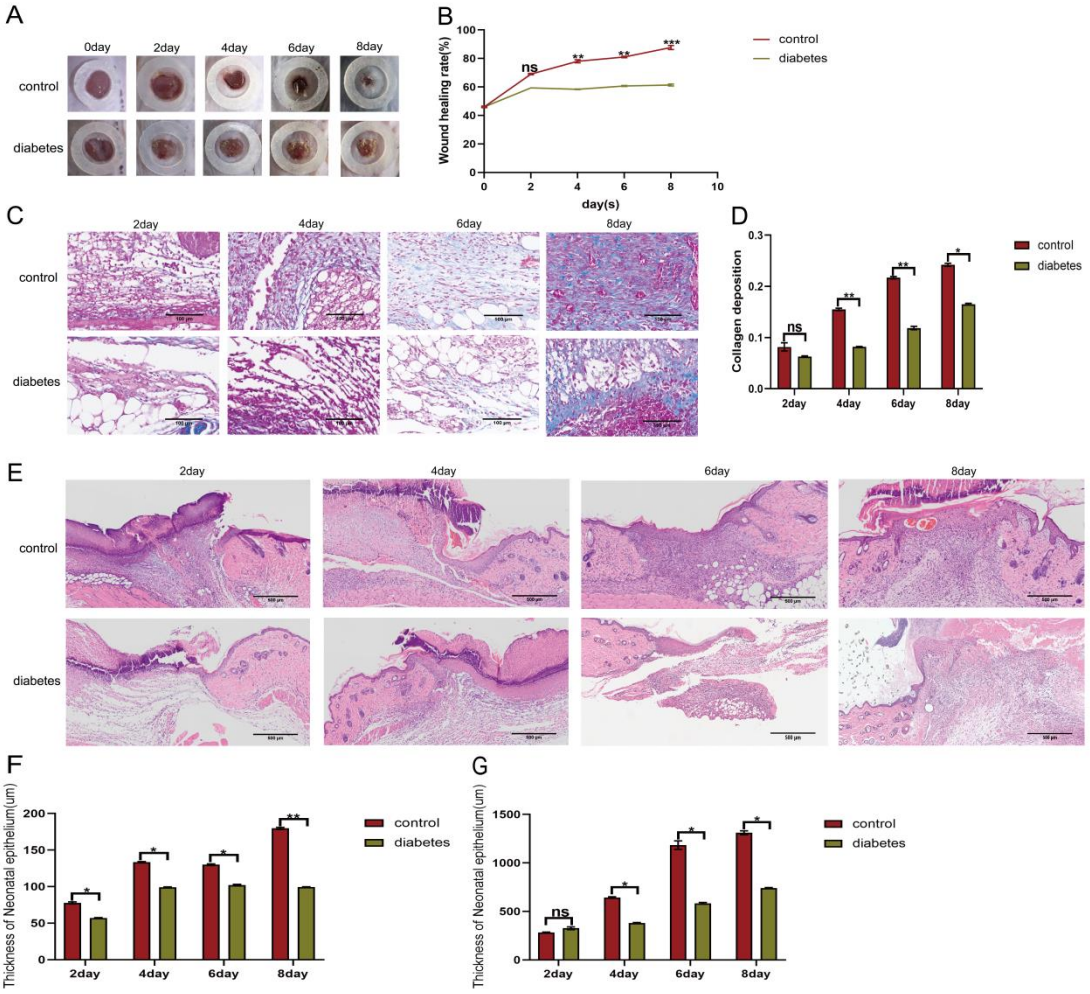


**Figure 1. Comparison of stained pathological sections between diabetic model mice and control model mice.** (A) Gross observation images of full thickness skin defect models for both diabetic and control mice at days 2, 4, 6, and 8 . (B) Statistical comparison of wound healing rates at four different time points between the two groups. (C) Masson staining comparison of collagen deposition in both groups at four time points. (D) Quantitative analysis of the wound collagen content. (E) H&E staining of pathological tissue sections from both groups on days 2, 4, 6 and 8. (F) Quantitative analysis of the thickness of the newly formed epithelial tongue. (G) Quantitative analysis of the length of the newly formed epithelial tongue. All the data are expressed as the mean ± SEM, with n = 3 independent biological replicates. P values were determined via an unpaired t-test (ns = not statistically significant; * $P < 0.05$; ** $P < 0.01$; *** $P < 0.001$).

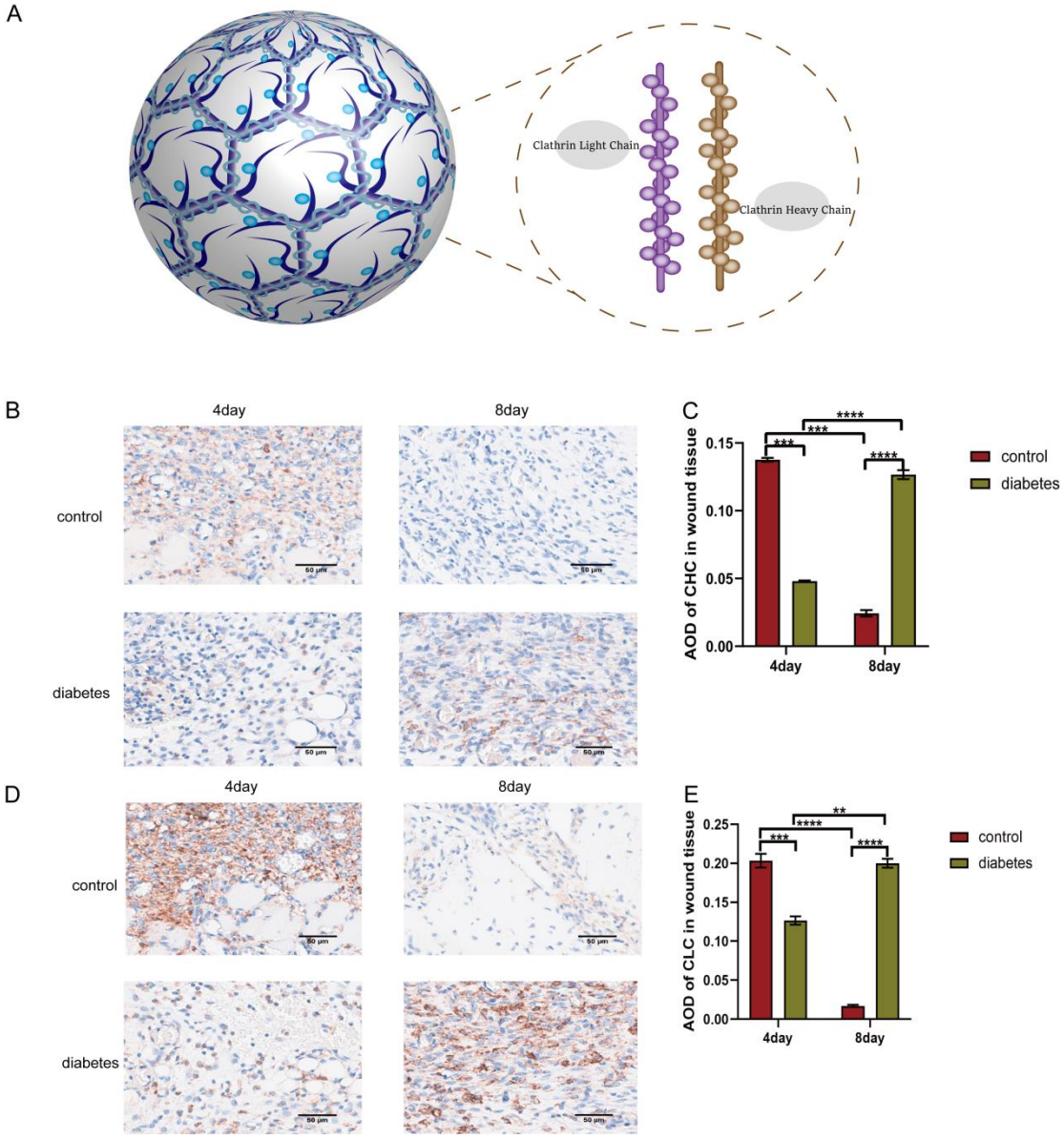


**Figure 2. Immunohistochemical staining of pathological sections.** (A)Schematic diagram of the clathrin protein structure. (B)Staining expression of the CHC in the sections. (C)Quantitative analysis of the expression levels of the CHC molecules on days 4 and 8 . (D)Staining expression of the CLC molecules in the sections. (E)Quantitative analysis of the expression levels of the CLC molecules on days 4 and 8 . The data are expressed as the mean ± SEM, with n = 3 independent biological replicates. P values were determined via an unpaired t-test (** P < 0.01; *** P < 0.001;****p<0.0001).CHC,clathrin heavy chain;CLC,clathrin light chain.

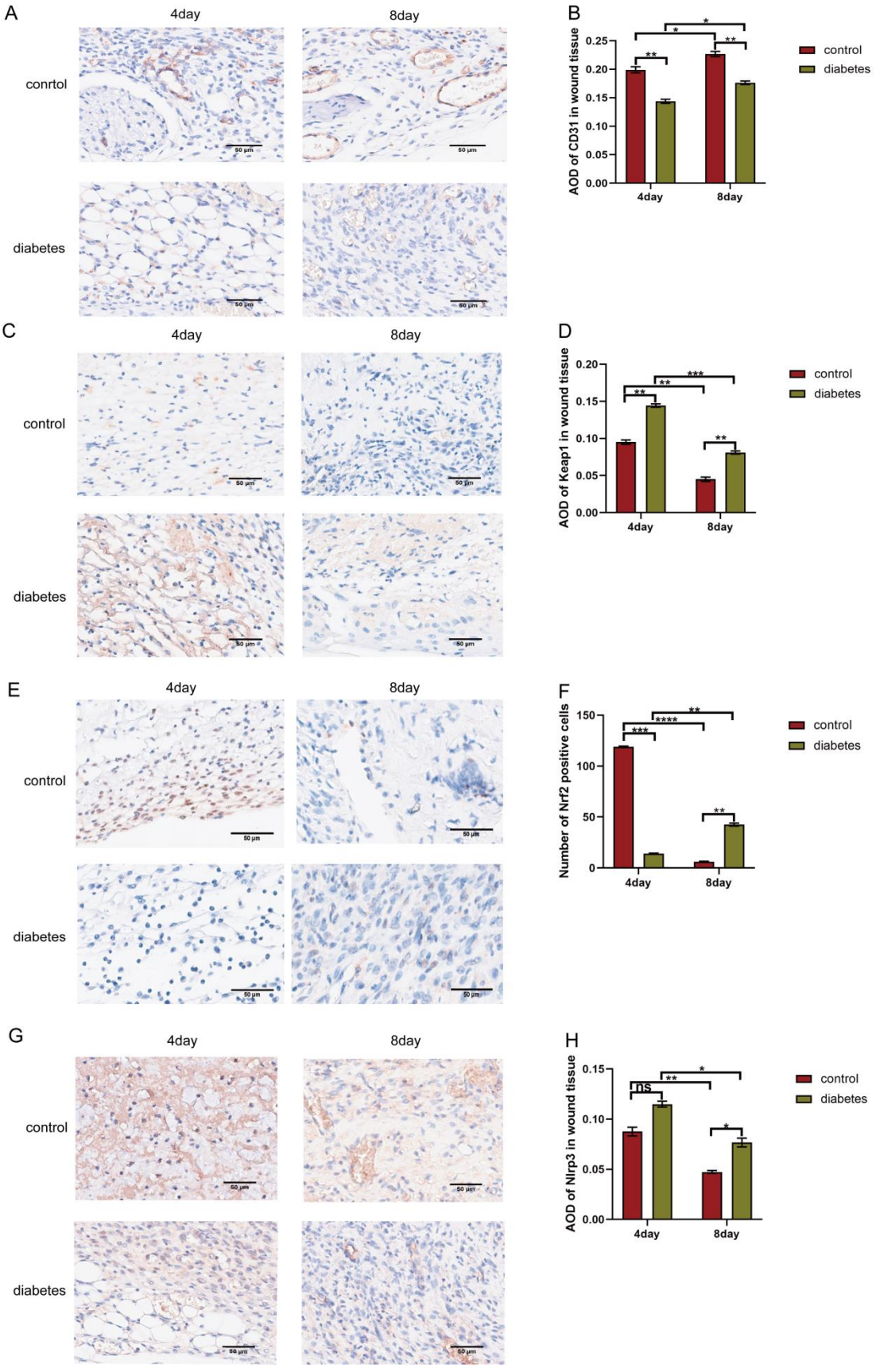


**Figure 3. Immunohistochemical staining of pathological sections.** (A), CD31 expression in the

sections. (B) Quantitative analysis and statistical comparison of CD31 expression levels on 4 and 8 day. (C) Keap1 expression in the sections. (D) Quantitative analysis and statistical comparison of Keap1 expression levels on days 4 and 8 . (E) Nrf2 expression in the sections. (F) Quantitative analysis and statistical comparison of Nrf2 expression levels on days 4 and 8 .(G) Nlrp3 expression in the sections. (H) Quantitative analysis and statistical comparison of Nlrp3 expression levels on days 4 and 8 . All the data are expressed as the mean ± SEM, with n = 3 independent biological replicates. P values were determined via an unpaired t-test (ns = not statistically significant; * P < 0.05; ** P < 0.01; *** P < 0.001;****p<0.0001). CD, cluster of differentiation; keap1, kelch like ech associated protein 1; Nrf2, nuclear factor erythroid 2 related factor 2; Nlrp3,nod like receptor thermal protein domain associated protein 3 .

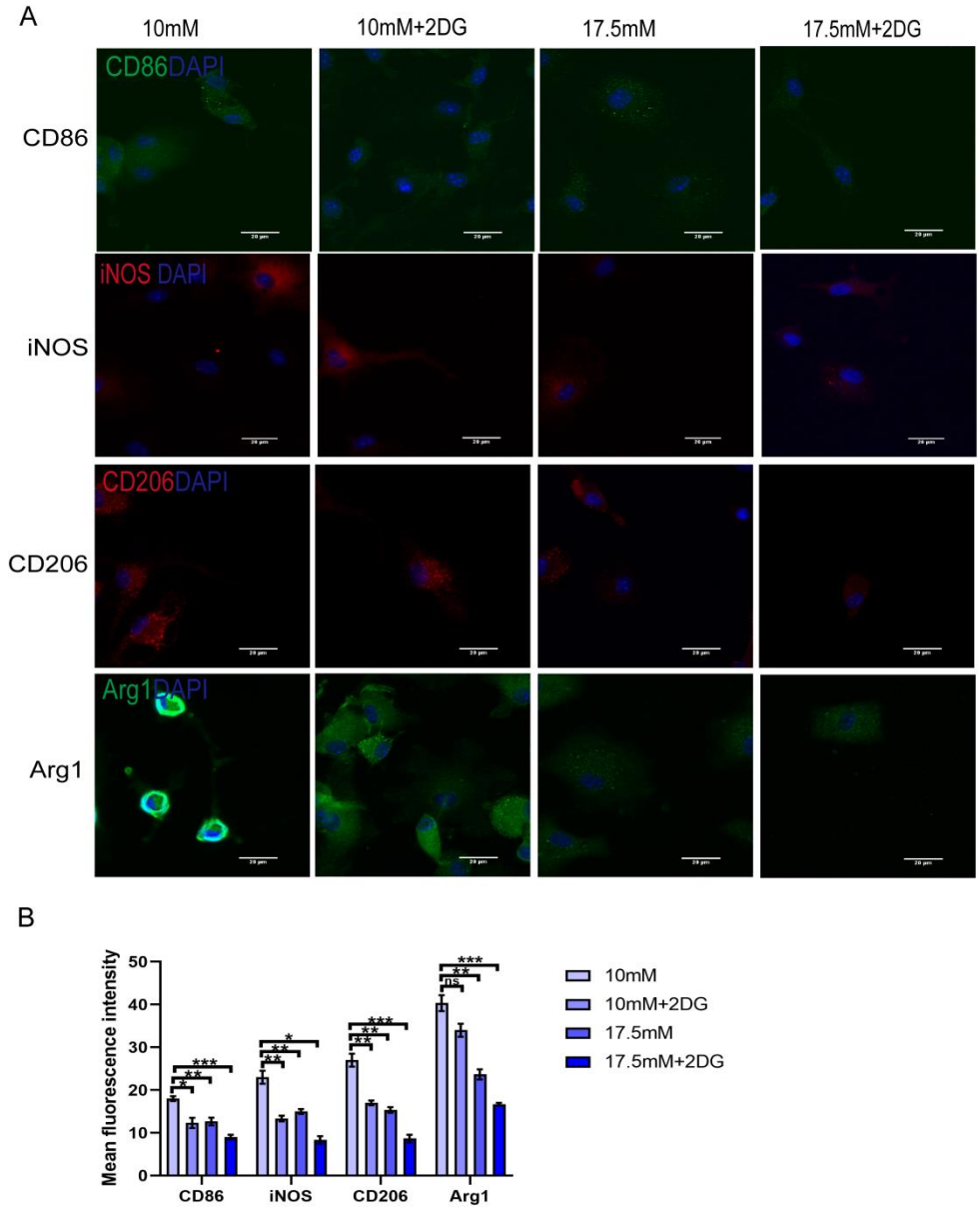


**Figure 4. Primary macrophage polarization responses.** (A) RTFQ-PCR of the CD86, iNOS, CD206, and Arg1 proteins was performed to assess the polarization of primary macrophages after stimulation. (B) Quantitative analysis of the fluorescence intensity of each protein. All the data are expressed as the mean ± SEM, with n = 3 independent biological replicates. P values were determined via an unpaired t-test (ns = not statistically significant; * P < 0.05; ** P < 0.01; *** P < 0.001). CD, cluster of differentiation; iNOS, inducible nitric oxide synthase; Arg1, arginase 1.

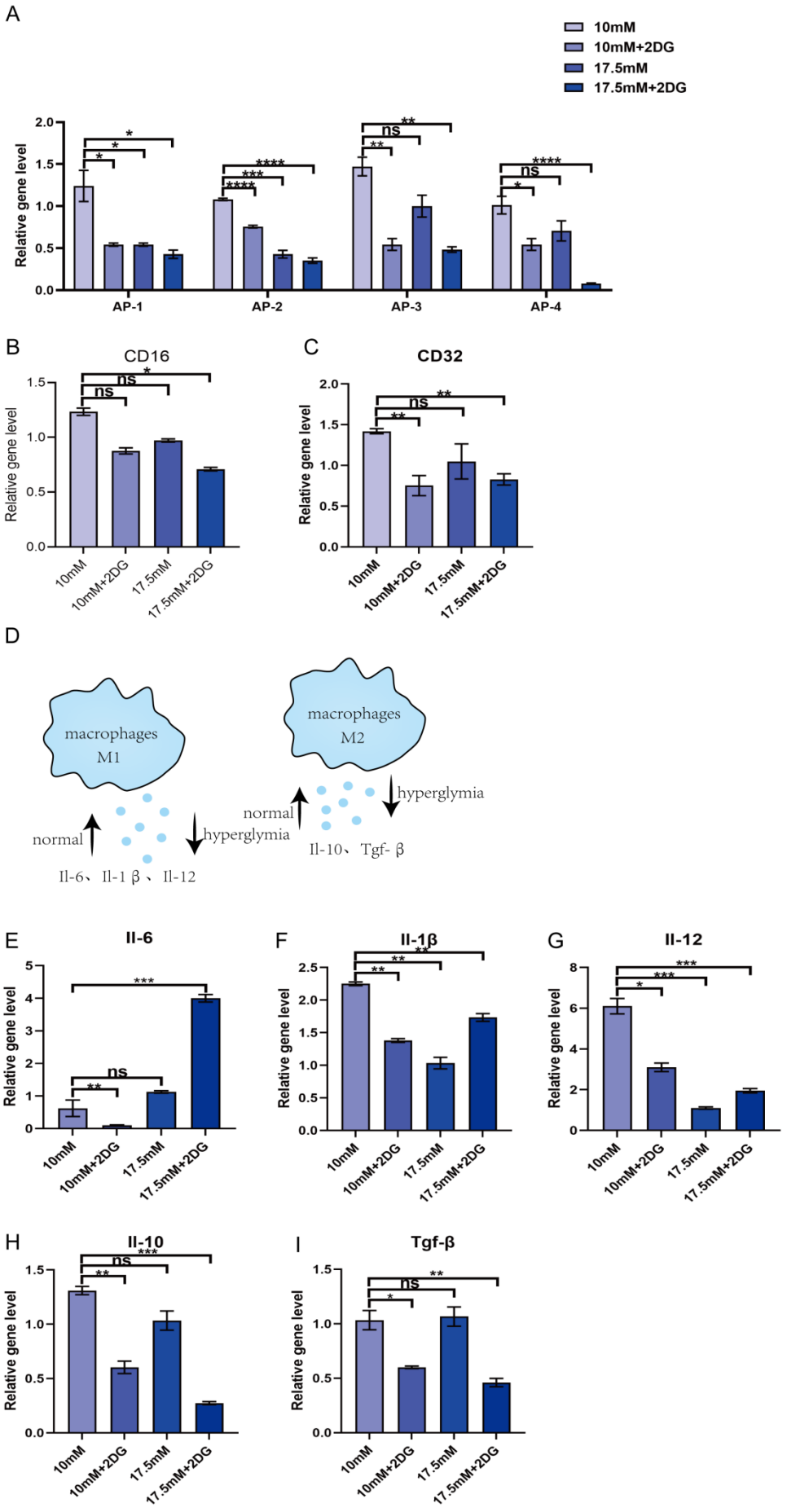
A
10mM
10mM+2DG
17.5mM
17.5mM+2DG
Relative gene level
AP-1
AP-2
AP-3
AP-4
B
CD16
C
CD32
D
macrophages M1
macrophages M2
normal
hyperglymia
Il-6、Il-1 β 、Il-12
Il-10、Tgf- β
E
Il-6
F
Il-1β
G
Il-12
H
Il-10
I
Tgf-β

**Figure 5. Macrophage secretion and surface receptor detection.** (A)Gene expression levels of the linker proteins AP-1, AP-2, AP-3, and AP-4 were measured under four different treatments using RTFQ-PCR.(B)The gene expression of CD16 in response to the four treatments was measured via RTFQ-PCR(C)The gene expression of CD32 in response to the four treatments was measured via RTFQ-PCR(D) Changes in the secretion of inflammatory cytokines by macrophages under normal conditions, high glucose, and impaired glucose utilization conditions. (E) Gene expression of Il-6 in response to the four treatments was measured via RTFQ-PCR(F) Gene expression of Il-1 β in response to the four treatments was measured via RTFQ-PCR (G)Gene expression of Il-12 in response to the four treatments was measured via RTFQ-PCR (H)Gene expression of Il-10 in response to the four treatments was measured via RTFQ-PCR.(I)Gene expression of Tgf- β in response to the four treatments was measured via RTFQ-PCR . All the data are expressed as the mean ± SEM, with n = 3 independent biological replicates. P values were determined via unpaired t-tests (ns = not statistically significant; *P < 0.05; **P < 0.01; ***P < 0.001; ****P < 0.0001). AP, adaptor protein; CD, cluster of differentiation; Il, interleukin; Tgf, transforming growth factor.

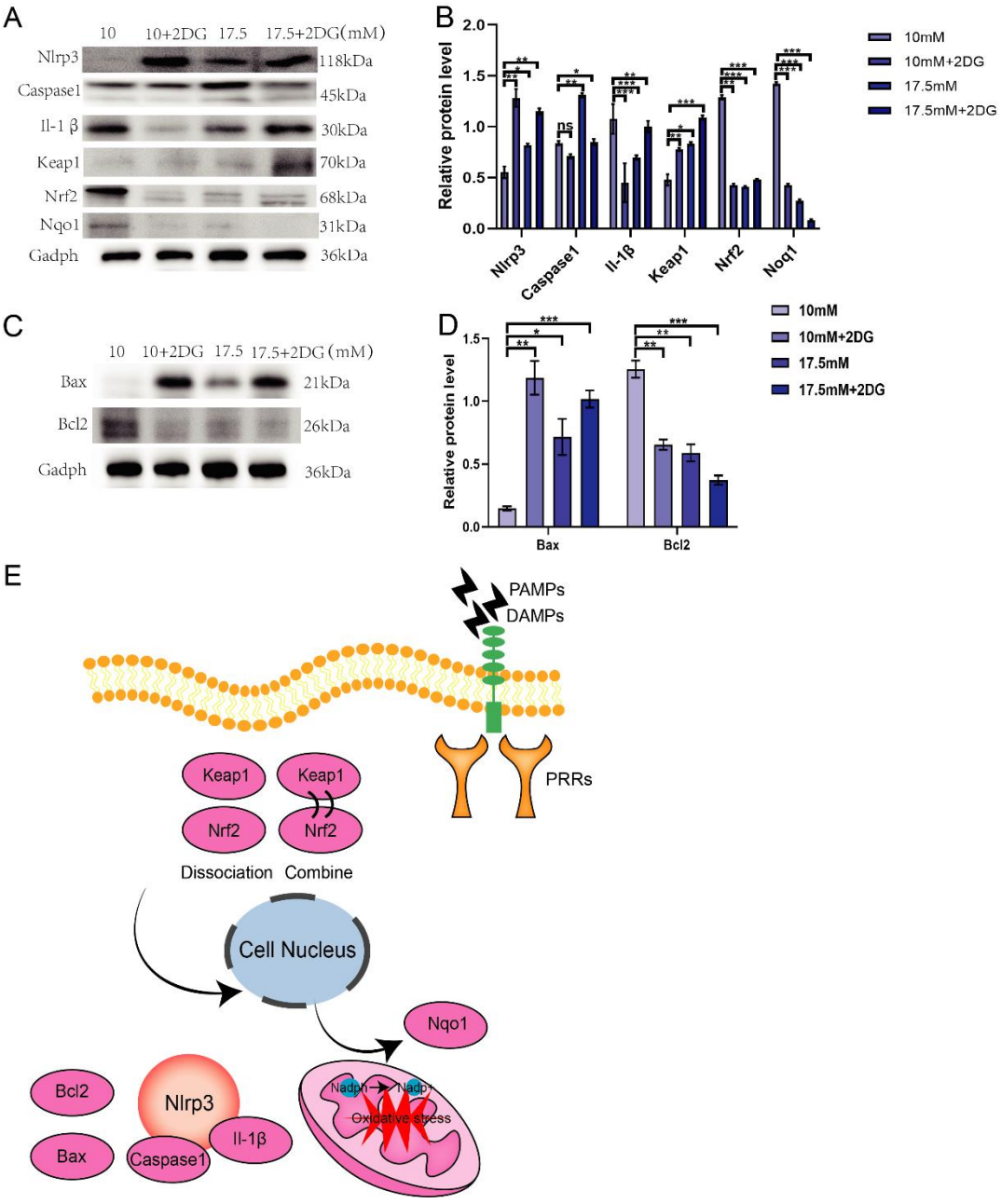


**Figure 6.The expression of specific proteins.** (A)WB was used to detect the expression bands of the inflammasome proteins Nlrp3, Caspase1, and Il-1 β , as well as the oxidative stress proteins

Keap1, Nrf2, and Nqo1. (B) Quantitative analysis of the expression levels of the inflammasome proteins Nlrp3, Caspase1, and Il-1 β and the oxidative stress proteins Keap1, Nrf2, and Nqo1. (C) WB was used to detect the expression of the apoptosis related proteins Bax and Bcl2. (D)Quantitative analysis was conducted on the expression levels of the apoptosis related proteins Bax and Bcl2. (E)A schematic diagram of the signal molecule pathways is presented. All the data are expressed as the mean ± SEM, n = 3 independent biological replicates. P values were determined via an unpaired t-test (ns = not significant; * $P < 0.05$; ** $P < 0.01$; *** $P < 0.001$). Nlrp3,nod like receptor thermal protein domain associated protein 3;Caspase1，cysteine aspartate protease 1；Il, interleukin; Keap1, kelch like ech associated protein 1; Nrf2, nuclear factor erythroid 2 related factor 2; Nqo1,nad(p)h:quinone oxidoreductase I; Bax, bcl2 associated x protein; Bcl2,b cell lymphoma 2;Gadph,glyceraldehydes 3 phosphatedehydrogenase;PAMPs, pathogen associated molecular patterns; DAMPs, damage associated molecular patterns; PRRs, pattern recognition receptors.

## References

[1]Knox S, O'Boyle NM. Skin lipids in health and disease: A review. *Chem Phys Lipids*. 2021;236:105055.

[2]Prost-Squarcioni C. Histologie de la peau et des follicules pileux [Histology of skin and hair follicle]. *Med Sci (Paris)*. 2006;22(2):131-137.

[3]Kloc M, Ghobrial RM, Wosik J, Lewicka A, Lewicki S, Kubiak JZ. Macrophage functions in wound healing. *J Tissue Eng Regen Med*. 2019;13(1):99-109.

[4] Louiselle AE, Niemiec SM, Zgheib C, Liechty KW. Macrophage polarization and diabetic wound healing. *Transl Res*. 2021;236:109-116.

[5]Fu X. Wound healing center establishment and new technology application in improving the wound healing quality in China. *Burns Trauma*. 2020;8:tkaa038.

[6]Abate MCMO, Aroucha PMT, Nóbrega DVMD, Rocha IPM, Soares SD, Reis AA, Paliares IC, Giuffrida FMA, Dib SA, Reis AF, Sa JR. Cutaneous manifestations of diabetes mellitus: a narrative review. Einstein (Sao Paulo). 2025 Mar 17;23:eRW1193.

[7]Abdelhakeem E, Monir S, Teaima MHM, Rashwan KO, El-Nabarawi M. State-of-the-Art Review of Advanced Electrospun Nanofiber Composites for Enhanced Wound Healing. *AAPS PharmSciTech*. 2023;24(8):246.

[8]He S, Cao H, Thålin C, Svensson J, Blombäck M, Wallén H. The Clotting Trigger Is an Important Determinant for the Coagulation Pathway In Vivo or In Vitro-Inference from Data Review. *Semin Thromb Hemost*. 2021;47(1):63-73.

[9] Afshar-Kharghan V, Thiagarajan P. Leukocyte adhesion and thrombosis. *Curr Opin Hematol*. 2006;13(1):34-39.

[10] Suzuki K. Chronic Inflammation as an Immunological Abnormality and Effectiveness of Exercise. *Biomolecules*. 2019;9(6):223.

[11]Ahmad I, Naqvi RA, Valverde A, Naqvi AR. LncRNA MALAT1/microRNA-30b axis regulates macrophage polarization and function. *Front Immunol*. 2023;14:1214810.

[12]Hassanshahi A, Moradzad M, Ghalamkari S, Fadaei M, Cowin AJ, Hassanshahi M. Macrophage-Mediated Inflammation in Skin Wound Healing. *Cells*. 2022;11(19):2953.

[19]Gerhardt H, Golding M, Fruttiger M, et al. VEGF guides angiogenic sprouting utilizing endothelial tip cell filopodia. *J Cell Biol*. 2003;161(6):1163-1177.

[20]Orzechowski A, Cywińska A, Rostagno AA, Rizzi FM. Oxidative Stress, Chronic Inflammation, and Amyloidoses. *Oxid Med Cell Longev*. 2019;2019:6024975.

[21]Atri C, Guerfali FZ, Laouini D. Role of Human Macrophage Polarization in Inflammation during Infectious Diseases. *Int J Mol Sci*. 2018;19(6):1801.

[22]Liu F, Qiu H, Xue M, Zhang S, Zhang X, Xu J.MSC-secreted Tgf-β regulates lipopolysaccharide-stimulated macrophage M2-like polarization via the Akt/FoxO1 pathway. *Stem Cell Res Ther*. 2019;10(1):345.

[23]Irizarry-Caro RA, McDaniel MM, Overcast GR, Jain VG, Troutman TD, Pasare C. TLR signaling adapter BCAP regulates inflammatory to reparatory macrophage transition by promoting histone lactylation. *Proc Natl Acad Sci U S A*. 2020;117(48):30628-30638.

[24]Barnes JA, Eid MA, Creager MA, Goodney PP. Epidemiology and Risk of Amputation in Patients With Diabetes Mellitus and Peripheral Artery Disease. Arterioscler Thromb Vasc Biol. 2020 Aug;40(8):1808-1817.

[25]Gerber PA, Rutter GA. The Role of Oxidative Stress and Hypoxia in Pancreatic Beta-Cell Dysfunction in Diabetes Mellitus. Antioxid Redox Signal. 2017 Apr 1;26(10):501-518.

[26]Cai F, Wang P, Chen W, Zhao R, Liu Y. The physiological phenomenon and regulation of macrophage polarization in diabetic wound. *Mol Biol Rep*. 2023;50(11):9469-9477.

[27] Zheng S, Zeng Y, Chu L, Gong T, Li S, Yang M. Renal Tissue-Derived Exosomal miRNA-34a in Diabetic Nephropathy Induces Renal Tubular Cell Fibrosis by Promoting the Polarization of M1 Macrophages. *IET Nanobiotechnol*. 2024;2024:5702517.

[28]Marro BS, Legrain S, Ware BC, Oldstone MB. Macrophage IFN-I signaling promotes autoreactive T cell infiltration into islets in type 1 diabetes model. JCI Insight. 2019 Jan 24;4(2):e125067.

[29]Wolf SJ, Melvin WJ, Gallagher K. Macrophage-mediated inflammation in diabetic wound repair. *Semin Cell Dev Biol*. 2021;119:111-118.

[30]Zheng J, Hu Q, Zou X, Xu G, Cao Y. Uranium induces kidney cells pyroptosis in culture involved in ROS/Nlrp3/Caspase1 signaling. *Free Radic Res*. 2022;56(1):40-52.

[31]Bai B, Yang Y, Wang Q, et al. Nlrp3inflammasome in endothelial dysfunction. *Cell Death Dis*. 2020;11(9):776.

[32]MUKHERJEE S, GHOSH R N, MAXFIELD F K. Endocytosis [ J] . Physiological Review , 1997, 77: 759-803.

[33]KIRCHHAUSEN T. Clathrin [ J] . Annual Review Biochemistry, 2000, 69: 699-727 .